Nano Research
2019, 12(12): 3037–3043
ISSN 1998-0124 CN 11-5974/O4
https://doi.org/10.1007/s12274-019-2549-7

Research Article

Radioiodinated tyrosine based carbon dots with efficient renal clearance for single photon emission computed tomography of tumor

Nian Liu[1,2,3,§], Yiyue Shi[1,§], Jingru Guo[1], Hai Li[4], Qiang Wang[5], Menglin Song[3], Zhiyuan Shi[3], Le He[4], Xinhui Su[5], Jin Xie[6], and Xiaolian Sun[1] (✉)

[1] *State Key Laboratory of Natural Medicines, Key Laboratory of Drug Quality Control and Pharmacovigilance, Department of Pharmaceutical Analysis, China Pharmaceutical University, Nanjing 210009, China*
[2] *Institute of Biological and Medical Imaging, Helmholtz Zentrum München and Technische Universität München, Neuherberg 85764, Germany*
[3] *State Key Laboratory of Molecular Vaccinology and Molecular Diagnostics & Center for Molecular Imaging and Translational Medicine, School of Public Health, Xiamen University, Xiamen 361005, China*
[4] *Institute of Functional Nano & Soft Materials (FUNSOM), Jiangsu Key Laboratory for Carbon-Based Functional Materials & Devices, Soochow University, Suzhou 215123, China*
[5] *Department of Nuclear Medicine, Zhongshan Hospital Xiamen University, Xiamen 361004, China*
[6] *Department of Chemistry, Bio-Imaging Research Center, University of Georgia, Athens, Georgia 30602, USA*
[§] *Nian Liu and Yiyue Shi contributed equally to this work.*

Received: 20 September 2019 / **Revised:** 18 October 2019 / **Accepted:** 21 October 2019

ABSTRACT

Nanoparticles with effective tumor accumulation and efficient renal clearance have attracted significant interests for clinical applications. We prepared 2.5 nm tyrosine based carbon dots (TCDs) with phenolic hydroxyl groups on the surface for directly ^{125}I labeling. The ^{125}I labeled polyethylene glycol (PEG) functionalized TCDs (^{125}I-TCDPEGs) showed excellent radiochemical stability both *in vitro* and *in vivo*. Due to the enhanced permeability and retention effect, these ^{125}I-TCDPEGs demonstrated a tumor accumulation around 4%–5% of the injected dose per gram (ID/g) for U87MG, 4T1, HepG2 and MCF7 tumor-bearing mice at 1 h post-injection. Meanwhile, the ^{125}I-TCDPEGs also could be fast renally excreted, with less than 0.6% ID/g left in the liver and spleen within 24 h. These radioactive carbon dots not only can be used for cellular fluorescence imaging due to their intrinsic optical property, but are also effective single photon emission computed tomography (SPECT) imaging agents for tumor. Together with their excellent biocompatibility and stability, we anticipate these ^{125}I-TCDPEGs of great potential for early tumor diagnosis in clinic. What's more, our TCDPEGs are also proved to be feasible carriers for other iodine isotopes such as ^{127}I and ^{131}I for different biomedical application.

KEYWORDS

radioiodination, tyrosine based carbon dots, single photon emission computed tomography (SPECT) imaging, fluoresecent imaging, renal clearance

1 Introduction

Nuclear medicine is one of the most widely used diagnostic tools in clinic. Combined with radioactive tracers, they enable noninvasive, highly sensitive and quantitative *in vivo* visualization of biological processes [1, 2]. A large amount of radiotracers have been developed for cancer diagnosis [3–6]. Radioiodine labeling is of great interest due to the availability of multiple radioactive iodine isotopes for nuclear medical applications, such as ^{125}I ($t_{1/2}$ =59.49 d) for single photon emission computed tomography (SPECT) imaging, ^{131}I ($t_{1/2}$ = 8.02 d) for radiotherapy and also the nonradioactive ^{127}I for X-ray computed tomography (CT) imaging [7, 8].

Various radioiodine labeled agents have been explored for tumor imaging. For biomolecules, the radioiodine labeling effectiveness is highly dependent on their structures and the radioiodination may significantly affect their biological activities and pharmacological properties [9–11]. The burgeoning growth of nanotechnology provides new opportunities for radioiodine delivery [12–15]. Radiolabeled nanomaterials have generally demonstrated excellent radiochemical stability and high tumor targeting capability due to the enhanced permeability and retention (EPR) effect. However, the nonspecific accumulation of nanomaterials in the reticuloendothelial system (RES) for weeks or even months, brings potential toxicity and radiation exposure concern. Therefore, the ultrasmall nanoparticles [16–18] or biodegradable nanoparticles [19–21] with the advantages of both tumor targeting and effective clearance have attracted more and more attentions.

Carbon dots (CDs) have unique optical properties, excellent stability and biocompatibility, holding great promise in the preclinical or potentially clinical applications [22, 23]. Most CDs studies have focused on their optical imaging application, which faces challenges such as low quantum yield of CDs and limited tissue penetration of light [24–27]. We have synthesized ultrasmall tyrosine based CDs (TCDs) simply via a hydrothermal reaction between L-tyrosine (Tyr) and citric acid (CA), and further modified them with PEG (Scheme 1). A standard Iodogen oxidation method results in nearly 100% radioiodine labeling yield, producing ^{125}I labeled TCDPEGs (^{125}I-TCDPEGs) with ultrahigh radiochemical stability both *in vitro* and

Address correspondence to xiaolian_sun@cpu.edu.cn

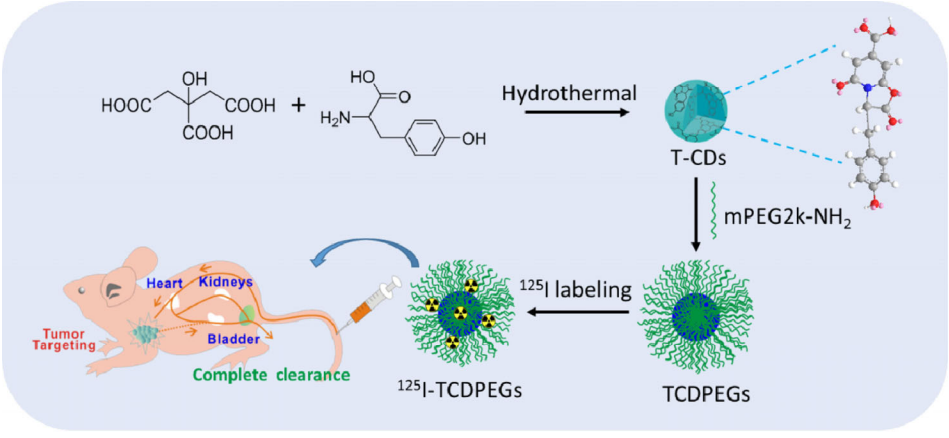

Scheme 1 An illustration of ^{125}I-TCDPEGs formation and *in vivo* application.

in vivo. ^{125}I-TCDPEGs showed pharmacokinetics analogous to small molecules and were fast cleared from the host within 24 h, meeting the demand by the U.S. Food and Drug Administration (FDA) on diagnostic agents applied into the human [28]. We were able to diagnose tumors in different (U87MG, 4T1, HepG2, and MCF7) tumor-bearing rodent models via SPECT imaging. Together with their excellent biocompatibility and stability, we expect these ^{125}I-TCDPEGs have the potential for clinical translation. Noteworthy, this iodine-labeling TCDPEGs strategy can be extended to other iodine isotopes such as ^{127}I and ^{131}I for different purposes.

2 Experimental

2.1 Materials and instrumentation

CA, Tyr, hydrochloric acid, dimethyl sulphoxide (DMSO), 1-ethyl-(3-dimethyllaminopropyl) carbodiie hydrochlide (EDC·HCl) and N-hydroxysuccinimide (NHS) were purchased from Aladdin Scientific Ltd. (Beijing, China). Methoxypolyethylene glycol amine (mPEG2k-NH_2, M_W = 2,000 Da) was purchased from Shanghai ToYong Biotech (Shanghai, China). Thiazolyl blue tetrazolium bromide (MTT), Dulbecco's modified Eagle's medium (DMEM), fetal bovine serum (FBS) and Penicilline-Streptomycin solution were purchased from HyClone Inc. High-resolution mass spectrometry was acquired from a Q Exactive LC-MS/MS system. ^{1}H and ^{13}C NMR spectra were performed on Bruker Avance II NMR spectrometer at 600 MHz with tetramethylsilane as the internal standard. Electron-spray ionization mass spectra in positive mode (ESI-MS) data were obtained on a Bruker Esquire 3000t spectrometer. Transmission electron microscopy (TEM) images and high resolution TEM images were recorded on a FEI Tecnai F20 TEM operating at 200 kV. Atomic force microscope (AFM) measurements were carrid out using a VeccoMultimode VNanoscope in the tapping mode. X-ray Photoelectron Spectroscopy (XPS) was performed using a KRATOS Axis Ultra-DLD X-ray photoelectron spectrometer with monochromatised Al Kα X-rays ($h\nu$ = 1,486.6 eV). UV–Vis absorption spectra were recorded on a UV-2550 (Shimadzu) spectrophotometer in the wavelength range of 190–900 nm. Fluorescent spectra were performed with a Hitachi F-4500 spectrometer. Fourier transform infrared (FTIR) spectra were characterized by Nicolet 380 FT-IR spectrometer. HPLC radiostability analysis was performed on Thermo Fisher Dionex UltiMate 3000 using the Nucleosil C18 (250 mm × 4 mm, 10 μm, 100 Å) column and chromatograms were collected at 254 nm wavelength.

2.2 Synthesis of TCD and TCDPEGs

CA (500 mg) and Tyr (410 mg) were added into 10 mL of deionized (DI) water, and mixed with 0.5 mL hydrochloric acid under vigorous stirring. Then the mixture was transferred into a 50 mL Teflon-lined stainless steel autoclave and heated at 200 °C for 5 h before cooled down to room temperature. The solution was further concentrated by centrifugation and purified via a silica gel column. The resulting TCDs (15 mg), EDC·HCl (30 mg), and NHS (30 mg) were then dissolved in 8 mL DMF, and stirred at room temperature for 2 h, before additional adding of mPEG2000-NH_2 (100 mg). After reacted at room temperature for 24 h, the organic solvent was evaporated to yield dark-brown crude product and was then purified by dialysis with DI water for 2 days.

2.3 ^{125}I-labeling

TCDPEGs were labeled with Na^{125}I using a standard Iodogen oxidation method. Typically, 100 μL of TCDPEGs (50 μg) and 500 μCi of Na^{125}I were added into an EP tube coated with Iodogen (20 μg). After shaking for 10 min, the solution was ready to use without further purification. ^{127}I labeling and ^{131}I labeling were carried out with the same method, but using 1 mg Na^{127}I or 500 μCi Na^{131}I instead.

2.4 Radiochemical stability

100 μL ^{125}I-TCDPEGs (20 μCi, 2 μg) were incubated in PBS (phosphate buffer saline) buffer (900 μL) and FBS (900 μL), respectively. Then 20 μL solution from PBS and FBS were taken out at different time points and analyzed via radio HPLC. The characteristic peak of free ^{125}I and ^{125}I-TCDPEGs came out at 3.7 and 15.8 min.

2.5 MTT assays

Cells (4T1, HepG2, MCF7, and U87MG) were seeded in a 96-well plate at a density of 1 × 10^4 cells/well for 24 h before treated with ^{125}I-TCDPEGs up to 40 μCi/4 μg. 10 μL of MTT solution was added after the cells were washed with PBS. After an additional 4 h incubation, the medium was aspirated and refilled with 100 μL DMSO. The relative viability (%) was referred to the ratio of the absorbance at 570 nm of experimental groups to that of the untreated groups.

2.6 Cellular internalization

A total of 1 × 10^4 of cells were seeded on glass dishes at 37 °C with 5% CO_2 atmosphere for 24 h. ^{125}I-TCDPEGs (20 μCi, 2 μg) were added into the dishes and incubated for 2 h. The cells were then rinsed with PBS for three times. The fluoresecence of TCDPEGs was observed by confocal microscope (Olympus, Japan). For the cellular uptake of radioactivity, the cells were lysed upon 1 M NaOH, then the suspended solutions were collected to the plastic tubes for radioactive γ-counter measurement.

2.7 SPECT imaging

All animal experiments reported herein were performed according to a protocol approved by the Xiamen University Institutional

Animal Care and Use Committee. The tumor models used were established upon subcutaneous injection of U87MG, 4T1, HepG2 and MCF7 cells (≈ 5 × 10^6) into female BALB/c nude mice (20–23 g) at the flank region of the hind leg. The tumor imaging studies were performed when the tumor size reached 5 mm.

SPECT/CT imaging of tumor-bearing Balb/c nude mice were obtained at 1, 2, 4, and 24 h after intravenous (i.v.) injected with 500 μCi/50 μg of ^{125}I-TCDPEGs using nanoScan SC (Mediso Medical Imaging System) equipped with pinhole collimator. The detailed scanning parameters were as following (scan time: 30 min; frame: 45; FOV: 26 mm × 26 mm × 70 mm; resolution: 0.4 mm). And the images were reconstructed and analyzed by Nucline software (Mediso Medical Imaging System). The tumor uptake is estimated by using a phantom signal of ^{125}I-TCDPEGs (500 μCi/50 μg) as a control and calibrated to be the counts in the tumor to the counts of phantom per gram of tissue.

2.8 CT imaging

The CT scanning was performed using Siemens Inveon device (Siemens Siemens Corp., Germany). For CT phantom experiments, ^{127}I-TCDPEGs and iohexol with concentrations of 0, 2.5, 5, 10, 25, 50, 100 mg/mL were placed in 200 μL tubes for test. For *in vivo* CT experiments, the Balb/c nude mice were subjected to CT scanning before and after intratumral injection. CT datas were acquired using an X-ray voltage biased to 50 kVp with a 670 μA anode current with projection angles of 720°.

2.9 Biodistribution study

The tumor-bearing mice were intravenously injected with ^{125}I-TCDPEGs at a dose of 500 μCi/50 μg. The organs or tissues such as blood, tumor, brain, muscle, bone, thyroid, heart, lung, liver, spleen, kidney, intestines, and stomach, were resected from the mice at 1, 2, 4, 8, and 24 h post-injection, wet-weighed, and put in plastic tubes for radioactive γ-counter measurement.

2.10 Biosafety evaluation

20 healthy mice were randomly divided into 4 groups randomly and i.v. injected with 100 μL saline for one group or ^{125}I-TCDPEGs at a dosage of 500 μCi/50 μg for the other 4 groups. The groups treated with ^{125}I-TCDPEGs were sacrificed at 2, 7, and 30 days, respectively. The blood samples were then collected for hematology and blood biochemistry test using automated analyzer (Hitachi-917, Hitachi). Major organs including heart, liver, spleen, lung and kidney were collected for hematoxylin and eosin (H&E) staining and histological examination.

3 Results and discussion

3.1 Synthesis and characterization of TCDs and TCDPEGs

TCDs were synthesized from CA and Tyr via a one-step hydrothermal reaction. The resulting TCDs were spherical, with a size of 2.42 ± 0.52 nm in TEM images (Fig. 1(a)). The AFM imaging further confirmed a topographic height of 2.53 ± 0.33 nm (Fig. 1(b)). The high-resolution TEM images indicated amorphous structures with no obvious lattice fringes. These TCDs exhibited a broad absorption with two major peaks at 240 and 280 nm (Fig. 1(e)), as well as excitation-wavelength dependent fluorescence (Fig. 1(f)). We assumed that the formation of TCDs involved at least two steps: the dehydration between CA and Tyr to produce an intermediate and

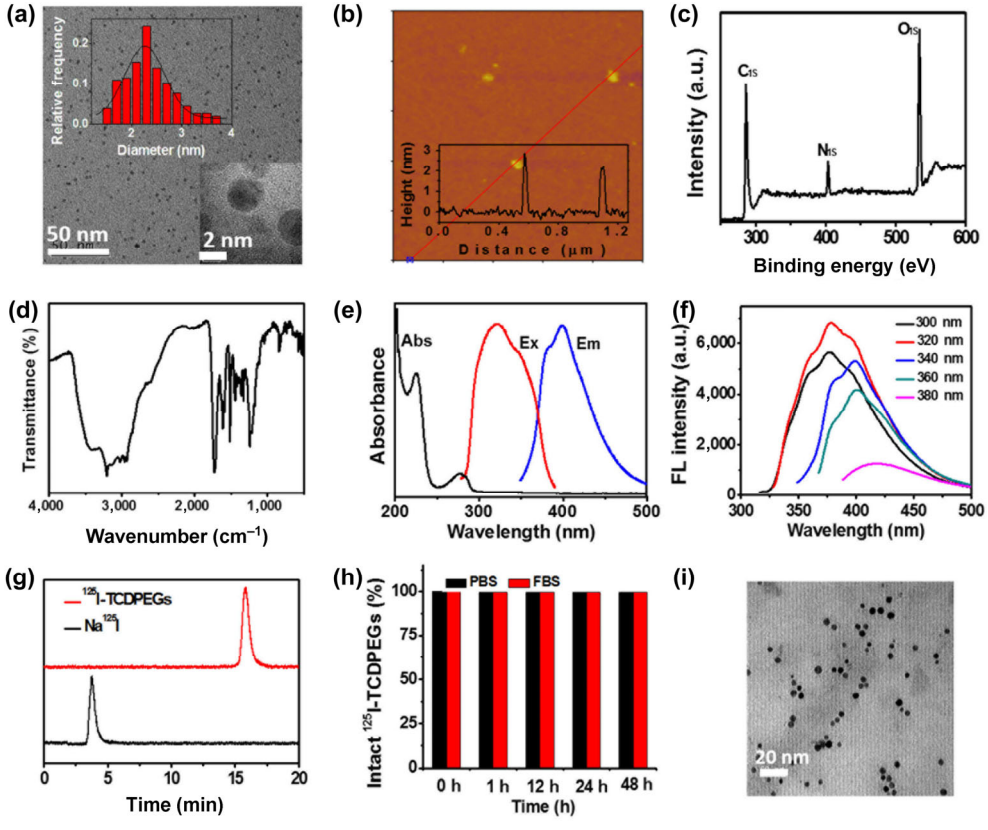

Figure 1 (a) TEM image of TCDs. Inset: diameter distribution and HRTEM of TCDs. (b) AFM image of TCDs. Inset: the height measured by AFM. (c) XPS survey of the TCDs. (d) FTIR spectrum of TCDs: C=C–H (1,515 and 1,613 cm^{-1}) bonds indicating the existence of phenyl structure; C=O (1,716 cm^{-1}) and OH (3,205 cm^{-1}) bonds indicating the existence of carboxylic group. (e) UV–Vis absorption (black, Abs), fluorescence excitation (red, Ex) and emission (blue, Em) spectra of TCDs. (f) Photoluminescence spectra of TCDs under excitation with light of different wavelengths. (g) Radio-HPLC chromatograms of ^{125}I-TCDPEGs. Na^{125}I solution was used as a control. (h) Radiolabeling stability of ^{125}I-TCDPEGs. No obvious intact ^{125}I was observed after incubation in PBS or 10% FBS at 37 °C for 2 days. (i) TEM of ^{125}I-TCDPEGs after ^{125}I decay.

the self-assembly of these intermediates into amorphous dots via π–π stacking (Scheme S1 in the Electronic Supplementary Material (ESM)). The XPS (Fig. 1(c)) confirmed the existence of C, N, O, with typical peaks for C 1s (285 eV), N 1s (400 eV), and O 1s (531 eV). The carboxyl and phenolic hydroxyl groups contained intermediates were identified by ESI-MS, ^{1}H NMR and ^{13}C NMR (Figs. S1–S3 in the ESM). FTIR spectrum (Fig. 1(d)) and the high-resolution XPS (Fig. S4 in the ESM) also confirmed the presence of these two groups in as-synthesized TCDs. These TCDs are well dispersed in DI water and PBS, showing no obvious aggregation for months. Since naked TCDs were cleared from the circulation too quickly for tumor imaging (Fig. S5 in the ESM), we then chemically conjugated amine-PEG on the carboxyl groups of TCDs to improve their circulation time. The successful PEGylation was confirmed by MALDI-TOF spectrum (Fig. S6 in the ESM), TEM (Fig. S7 in the ESM) and zeta potential analysis (Fig. S8 in the ESM). The hydrodynamic size of TCDPEGs was around 5 nm, based on the gel-filtration chromatography (GFC) analysis.

3.2 ^{125}I labeling of TCDPEGs

The ^{125}I labeling was carried out by a standard Iodogen oxidation method onto the phenolic hydroxyl groups of TCDPEGs [29]. A nearly 100% labeling yield was reached within 10 min (Fig. 1(g)) and no detachment of ^{125}I was observed when incubating ^{125}I-TCDPEGs in PBS or 10% FBS at 37 °C for over 48 h (Fig. 1(h)). The ^{125}I labeling did not cause obvious changes to the morphology or optical properties of TCDPEGs (Fig. 1(i) and Fig. S9 in the ESM).

3.3 *In vivo* stability and distribution of ^{125}I-TCDPEGs

The distribution of ^{125}I-TCDPEGs in normal Balb/c mice was evaluated. It's worth to mention that the detached iodine ions accumulated in the thyroid *in vivo* [30, 31]. As shown in Fig. 2, the ^{125}I-TCDPEGs exhibited excellent *in vivo* radiochemical stability with nearly no signal in the thyroid within 24 h. The radioactive signal quickly spread the whole body and dominated in the bladder and the kidneys within 1 h. After 4 h, the signal was dramastically decreased and was almost undetectable up to 24 h (Figs. 2(a)–2(c)). The organ distribution of radioactivity was measured by γ-counter 24 h post-injection. Around 2.5% of the injected dose per gram (ID/g) was left in the kidney, while less than 0.6% ID/g was left in other organs including blood, liver and spleen, validating the fast renal clearance of ^{125}I-TCDPEGs. A careful examination of the mouse urine and feces confirms the integrity of ^{125}I-TCDPEGs during circulation (Fig. 2(e)), with the radioactive elution maintained at 15 min. Besides, our ^{125}I-TCDPEGs showed a two-compartment pharmacokintics with a rapid $t_{1/2\alpha}$ of 54.0 min and a $t_{1/2\beta}$ of 3.4 h (Figs. 2(f) and 2(g)), similar with many small molecule imaging agents [32, 33].

3.4 Cellular uptake of ^{125}I-TCDPEGs

We then investigated the tumor uptake of ^{125}I-TCDPEGs. The intracellular uptake of ^{125}I-TCDPEGs by different tumor cells (4T1, HepG2, MCF7, and U87MG) was monitored by confocal microscopy. Intrinsic fluorescent properties of TCDPEGs (ex/em: 358/461 nm) was observed in the cytoplasm after 2 h incubation (Fig. 3(a)). The internalization efficiency of ^{125}I-TCDPEGs were much higher than that of free Na^{125}I in these four kinds of cells, as shown in Fig. 3(b). No cellular toxicity was observed even at a concentration up to 40 μCi/ 4 μg (Fig. 3(c)).

3.5 *In vivo* tumor SPECT imaging of ^{125}I-TCDPEGs

We then performed the *in vivo* SPECT imaging of ^{125}I-TCDPEGs (500 μCi / per mouse) in tumor bearing mice. Our ^{125}I-TCDPEGs showed a tumor accumulation starting around 4.65 ± 0.47% ID/g for U87MG tumor-bearing mice at 1 h (Fig. 4), slightly decreasing to 3.21 ± 0.41% ID/g at 2 h and then keeping decreasing within 24 h, with a similar behavior of the tumor receptor imaging probes [34] such as ^{125}I-c(RGDyK) (Fig. S10 in the ESM). *Ex vivo* fluorescence imaging further confirmed that the ^{125}I-TCDPEGs mainly distributed in the tumor, liver and kidney (Fig. S11 in the ESM). As a control, free Na^{125}I barely reached tumor tissues (Fig. S12 in the ESM). What's more, due to the EPR effect, the ^{125}I-TCDPEGs are proved to be an effective tumor diagnosis probe for 4T1, HepG2 and MCF7 tumor-bearing mice, with the tumor accumulation around 4.49 ± 0.52%, 4.24 ± 0.41%, and 4.17 ± 0.43% ID/g, respectively. The detailed biodistribution studies of ^{125}I-TCDPEGs at different time points (Fig. S13 in the ESM) further confirmed their tumor accumulation and effective clearance from tissues. It's worth to mention that the

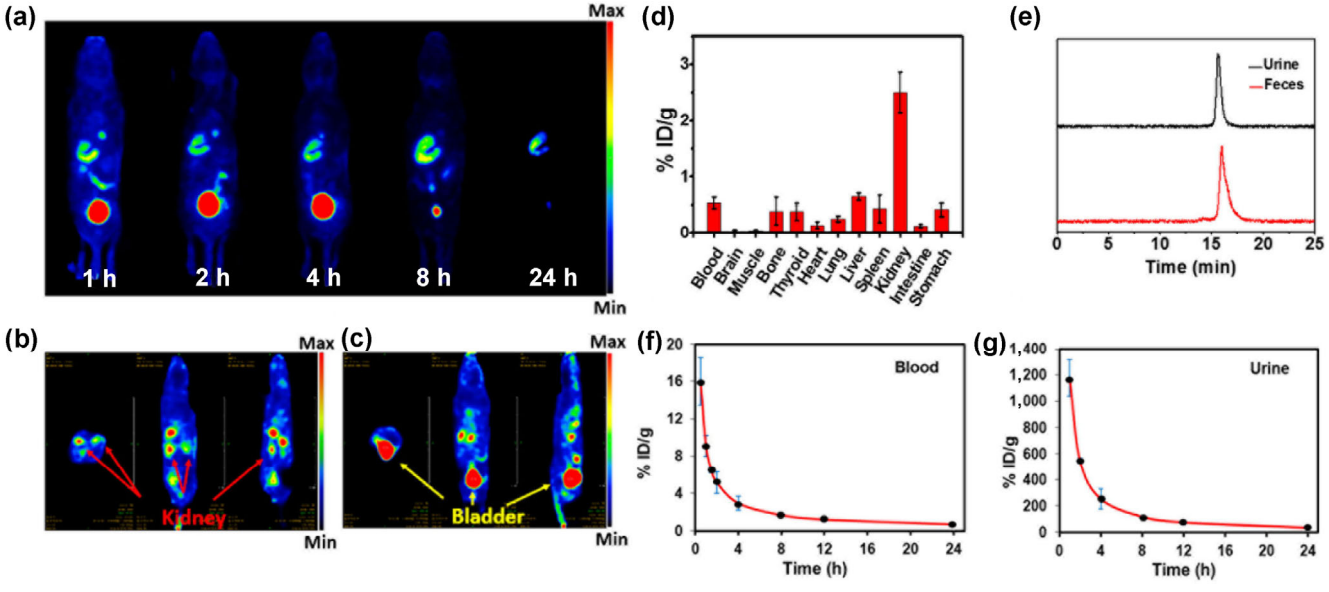

Figure 2 (a) Representative SPECT images at 1, 2, 4, 8, 24 h after i.v. injection of ^{125}I-TCDPEGs. (b) and (c) Representative SPECT 2D section images obtained at 2 h after i.v. injection of ^{125}I-TCDPEGs to show the kidneys (b) and the bladder (c) accumulation. Left to right: transverse, coronal, and sagittal views. (d) Biodistribution of ^{125}I-TCDPEGs 24 h after i.v. injection to mice (n = 5). (e) Radio-HPLC chromatograms of a urine sample and a feces sample taken from a mouse 4 h after ^{125}I-TCDPEGs injection. The radioactivity in collected sample barely can be detected after 4 h. (f) and (g) The time-dependent radioactivity curve of ^{125}I-TCDPEGs in the blood (f) and urine (g).

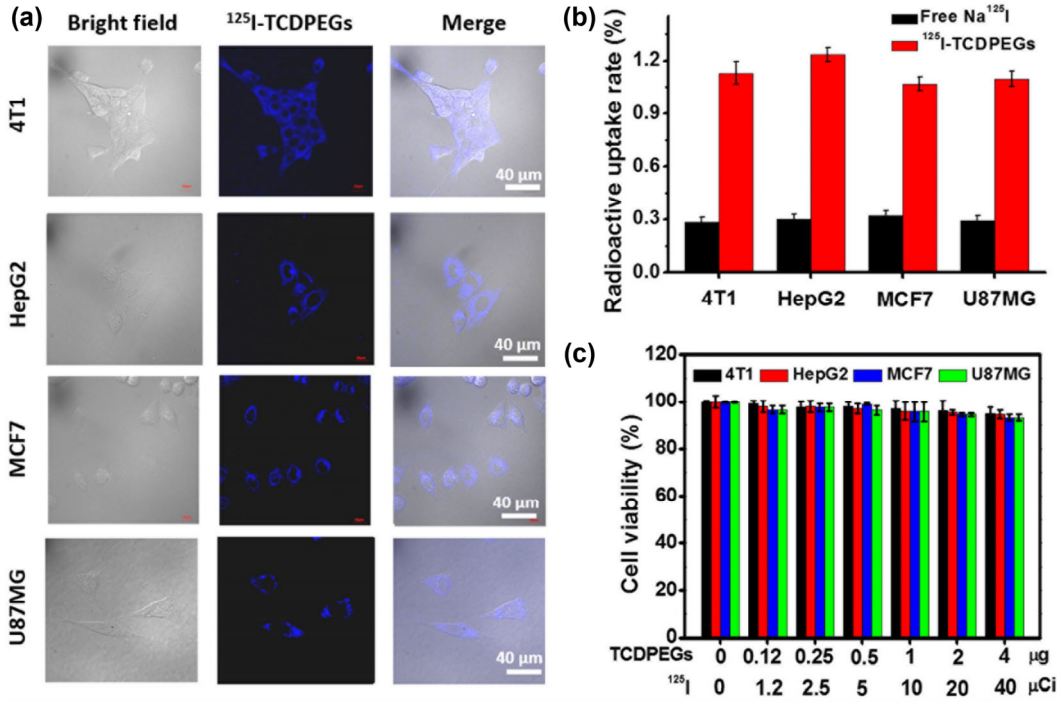

Figure 3 (a) Confocal images of 4T1, HepG2, MCF7 and U87MG cells incubated with ^{125}I-TCDPEGs for 2 h. (b) Cellular uptake of ^{125}I-TCDPEGs (20 μCi /2 μg) and Na^{125}I (20 μCi) at 2 h post-incubation. (c) Relative cell viabilities of 4T1, HepG2, MCF7 and U87MG cells after incubation with ^{125}I-TCDPEGs up to 40 μCi/4 μg for 24 h.

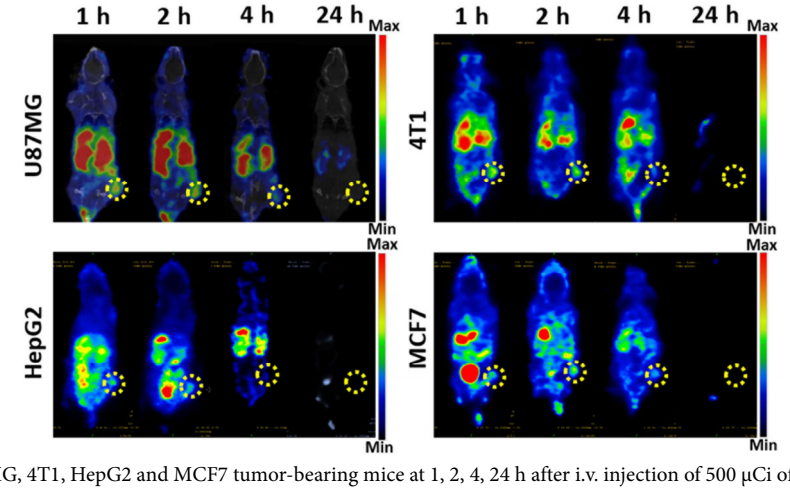

Figure 4 SPECT imaging of U87MG, 4T1, HepG2 and MCF7 tumor-bearing mice at 1, 2, 4, 24 h after i.v. injection of 500 μCi of ^{125}I-TCDPEGs.

normal tissue clearance efficiency of the ^{125}I-TCDPEGs is higher than many reported ultrasmall NPs [16–18] due to not only their small size, desired surface chemistry, but also the low density of carbon dots [35].

3.6 Biosafety evaluation of ^{125}I-TCDPEGs

Biosafety is of great significant for clinical translation of imaging probes [36]. To evaluate the safety of ^{125}I-TCDPEGs, healthy mice were injected with ^{125}I-TCDPEGs (500 μCi/50 μg). The mice were scarificed at 2, 7 and 30 d post-injection and blood smaples were collected for examination (n = 5) (Figs. 5(a) and 5(b)). All tested blood chemistry parameters and hematology analysis results demonstrated no significant difference between the ^{125}I-TCDPEGs treated mice and the control mice. The H&E staining and histology analysis of major organs (Fig. 5(c)) further confirmed that no noticeable inflammation or damage in any organs was induced by ^{125}I-TCDPEGs.

3.7 TCDPEGs as a general and facile carrier for iodination

We next evaluated the potential of TCDPEGs for other iodine delivery. TCDPEGs were successfully labeled with radioactive Na^{131}I and nonradioactive Na^{127}I via the same Iodogen oxidation method mentioned above, but using 500 μCi Na^{131}I or 1 mg Na^{127}I instead of 500 μCi Na^{125}I. The ^{131}I-TCDPEGs were also proved to be a SPECT imaging agent with high radiochemical stability (Fig. S14 in the ESM). The nonradioactive iodine loading of the TCDPEGs was determined to be around 30% and the ESI-MS spectrum proved the iodination of phenolic hydroxyl groups of TCDPEGs (Fig. S15 in the ESM). These ^{127}I-TCDPEGs demonstrated similar X-ray absorption capability with clinical used CT contrast agents, iohexol (Fig. 6). Strong CT signals in the tumor were detected after intratumoral injection of the ^{127}I-TCDPEG. Above results indicate that the TCDPEGs can serve as a general and facile carrier for iodination.

4 Conclusion

We prepared TCDs via a simple hydrothermal reaction between CA and Tyr. Compared with other iodine carriers, our TCDPEGs are easy to synthesize and afford high physicochemical stability. The TCDPEGs can be directly labeled with ^{125}I with ultrahigh efficiency and radiochemical stability. The labeling procedure only takes 10 min

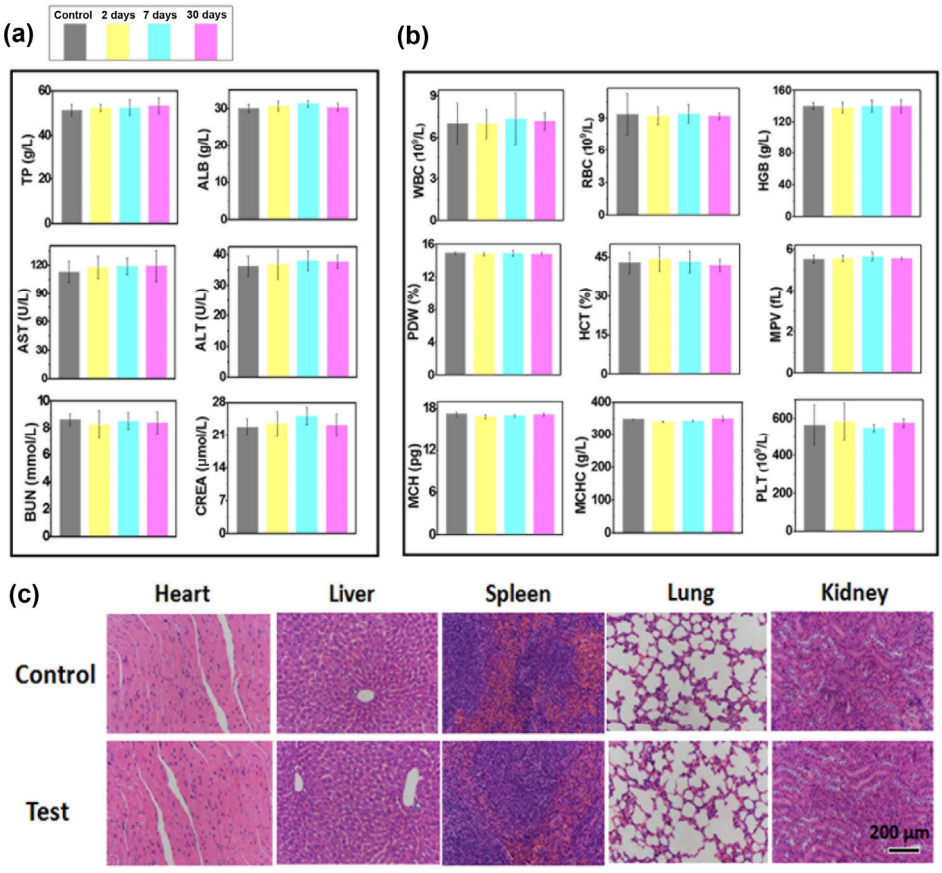

Figure 5 Blood biochemistry (a) and hematology (b) analysis datas of healthy mice 2, 7, 30 days after i.v. injection with ^{125}I-TCDPEGs (0.5 mg/mouse) or with PBS (control). TP, total protein; ALB, albumin; AST, aspartate transferase; ALT, alanine transferase; BUN, blood urea nitrogen; CREA, creatinine; WBC, white blood cells; RBC, red blood cells; HGB, hemoglobin; PDW; HCT, hematocrit; MPV, mean platelet volume; MCH, mean corpuscular hemoglobin; MCHC, mean corpuscular hemoglobin concentration. (c) H&E stained images of major organs of mice 2 d after treated with ^{125}I-TCDPEGs or with PBS.

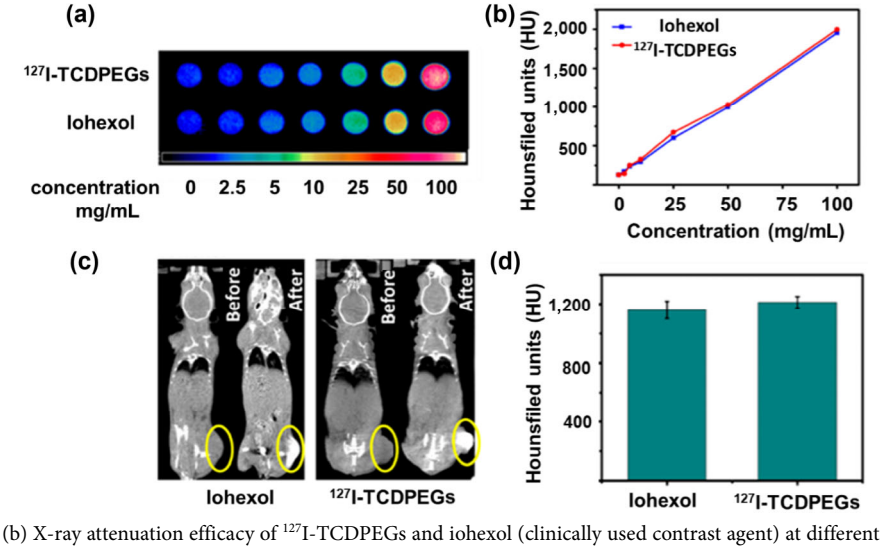

Figure 6 (a) CT imaging and (b) X-ray attenuation efficacy of ^{127}I-TCDPEGs and iohexol (clinically used contrast agent) at different concentrations. (c) CT imaging of a U87MG tumor-bearing mouse before (up) and after (down) intratumoral injection with 2 mg of ^{127}I-TCDPEGs. The CT contrast was obviously enhanced in the mouse tumor.

with 100% labeling yield, making it favorable for clinical uses. The ^{125}I-TCDPEGs exhibited small-molecule like pharmacokinetics and could be excreted within 24 h via renal clearance. The clearance effectiveness of ^{125}I-TCDPEGs is superior than many ultrasmall nanoparticles previously reported [16–18], with less than 0.6% ID/g liver accumulation within 24 h. Meanwhile, due to the EPR effect, their tumor imaging ability is comparable to many active targeting imaging probes, and applicable to a variety of tumor types regardless of their receptor. Given their excellent biocompatibility and stability, we anticipate these ^{125}I-TCDPEGs holding great potential for early tumor diagnosis in clinic. More importantly, the labeling approach can be easily extended to other iodine isotopes (^{127}I and ^{131}I) for different biomedical applications.

Acknowledgements

X. S. acknowledges the National Key Research and Development Program of China (No. 2016YFA0203600), the National Natural

Science Foundation of China (Nos. 81971738 and 81571743), the Project Program of State Key Laboratory of Natural Medicines, and the China Pharmaceutical University (No. SKLNMZZRC05).

Notes

The authors declare no competing financial interest.

Electronic Supplementary Material: Supplementary material (detailed characteristics of TCDs (^{1}H NMR, ^{13}C NMR, high resolution XPS spectra, MALDI-TOF spectrum, TEM, zeta potential, fluorescence spectra measurement of TCDs), SPECT imaging of ^{125}I-TCDPEGs, ^{125}I-c(RGDyK) and Na^{125}I, biodistribution of ^{125}I-TCDPEGs, *ex vivo* fluorescence imaging of major organs, ESI-MS spectrum of ^{127}I labeled TCDs, CT imaging of ^{127}I labeled TCDs) is available in the online version of this article at https://doi.org/10.1007/s12274-019-2549-7.

References

[1] Charlton, K. A sustainable future for nuclear imaging. *Nat. Rev. Phys.* **2019**, *1*, 530–532.

[2] Zeglis, B. M.; Holland, J. P.; Lebedev, A. Y.; Cantorias, M. V.; Lewis, J. S. Radiopharmaceuticals for imaging in oncology with special emphasis on positron-emitting agents In *Nuclear Oncology: Pathophysiology and Clinical Applications*. Strauss, H. W.; Mariani, G.; Volterrani D.; Larson S. M., Eds.; Springer: New York, 2013; pp 35–78.

[3] Dunphy, M. P.; Lewis, J. S. Radiopharmaceuticals in preclinical and clinical development for monitoring of therapy with PET. *J. Nucl. Med.* **2009**, *50 Suppl 1*, 106S–121S.

[4] Park, S. M.; Aalipour, A.; Vermesh, O.; Yu, J. H.; Gambhir, S. S. Towards clinically translatable *in vivo* nanodiagnostics. *Nat. Rev. Mater.* **2017**, *2*, 17014.

[5] Sun, X. L.; Cai, W. B.; Chen, X. Y. Positron emission tomography imaging using radiolabeled inorganic nanomaterials. *Acc. Chem. Res.* **2015**, *48*, 286–294.

[6] Pampaloni, M. H.; Nardo, L. PET/MRI radiotracer beyond ^{18}F-FDG. *PET Clin.* **2014**, *9*, 345–349.

[7] Mushtaq, S.; Jeon, J.; Shaheen, A.; Jang, B. S.; Park, S. H. Critical analysis of radioiodination techniques for micro and macro organic molecules. *J. Radioanal. Nucl. Chem.* **2016**, *309*, 859–889.

[8] Cavina, L.; van der Born, D.; Klaren, P. H. M.; Feiters, M. C.; Boerman, O. C.; Rutjes, F. P. J. T. Design of radioiodinated pharmaceuticals: Structural features affecting metabolic stability towards *in vivo* deiodination. *Eur. J. Org. Chem.* **2017**, *2017*, 3387–3414.

[9] Seevers, R. H.; Counsell, R. E. Radioiodination techniques for small organic molecules. *Chem. Rev.* **1982**, *82*, 575–590.

[10] Bailey, G. S. Labeling of peptides and proteins by radioiodination. In *Basic Protein and Peptide Protocols*; Walker, J. M., Ed.; Springer: Humana Press, 1994; pp 441–448.

[11] Dewanjee, M. K. Methods of radioiodination reactions with several oxidizing agents. In *Radioiodination: Theory, Practice, and Biomedical Applications*; Dewanjee, M. K., Ed.; Springer: Boston, MA, 1992; pp 129–218.

[12] Yi, X.; Xu, M. Y.; Zhou, H. L.; Xiong, S. S.; Qian, R.; Chai, Z. F.; Zhao, L.; Yang, K. Ultrasmall hyperbranched semiconducting polymer nanoparticles with different radioisotopes labeling for cancer theranostics. *ACS Nano* **2018**, *12*, 9142–9151.

[13] Song, M. L.; Liu, N.; He, L.; Liu, G.; Ling, D. S.; Su, X. H.; Sun, X. L. Porous hollow palladium nanoplatform for imaging-guided trimodal chemo-, photothermal-, and radiotherapy. *Nano Res.* **2018**, *11*, 2196–2808.

[14] Yi, X.; Yang, K.; Liang, C.; Zhong, X. Y.; Ning, P.; Song, G. S.; Wang, D. L.; Ge, C. C.; Chen, C. Y.; Chai, Z. F. et al. Imaging-guided combined photothermal and radiotherapy to treat subcutaneous and metastatic tumors using iodine-131-doped copper sulfide nanoparticles. *Adv. Funct. Mater.* **2015**, *25*, 4689–4699.

[15] Phillips, E.; Penate-Medina, O.; Zanzonico, P. B.; Carvajal, R. D.; Mohan, P.; Ye, Y. P.; Humm, J.; Gönen, M.; Kalaigian, H.; Schoder, H. et al. Clinical translation of an ultrasmall inorganic optical-PET imaging nanoparticle probe. *Sci. Transl. Med.* **2014**, *6*, 260ra149.

[16] Zhou, M.; Li, J. J.; Liang, S.; Sood, A. K.; Liang, D.; Li, C. CuS nanodots with ultrahigh efficient renal clearance for positron emission tomography imaging and image-guided photothermal therapy. *ACS Nano* **2015**, *9*, 7085–7096.

[17] Wen, L.; Chen, L.; Zheng, S. M.; Zeng, J. F.; Duan, G. X.; Wang, Y.; Wang, G. L.; Chai, Z. F.; Li, Z.; Gao, M. Y. Ultrasmall biocompatible WO_{3-x} nanodots for multi-modality imaging and combined therapy of cancers. *Adv. Mater.* **2016**, *28*, 5072–5079.

[18] Shen, S. D.; Jiang, D. W.; Cheng, L.; Chao, Y.; Nie, K. Q.; Dong, Z. L.; Kutyreff, C. J.; Engle, J. W.; Huang, P.; Cai, W. B. et al. Renal-clearable ultrasmall coordination polymer nanodots for chelator-free ^{64}Cu-labeling and imaging-guided enhanced radiotherapy of cancer. *ACS Nano* **2017**, *11*, 9103–9111.

[19] Chen, L.; Chen, J. Y.; Qiu, S. S.; Wen, L.; Wu, Y.; Hou, Y.; Wang, Y.; Zeng, J. F.; Feng, Y.; Li, Z. et al. Biodegradable nanoagents with short biological half-life for SPECT/PAI/MRI multimodality imaging and PTT therapy of tumors. *Small* **2018**, *14*, 1702700.

[20] Lu, N.; Fan, W. P.; Yi, X.; Wang, S.; Wang, Z. T.; Tian, R.; Jacobson, O.; Liu, Y. J.; Yung, B. C.; Zhang, G. F. et al. Biodegradable hollow mesoporous organosilica nanotheranostics for mild hyperthermia-induced bubble-enhanced oxygen-sensitized radiotherapy. *ACS Nano* **2018**, *12*, 1580–1591.

[21] Chen, D. Q.; Zhang, G. Q.; Li, R. M.; Guan, M. R.; Wang, X. Y.; Zou, T. J.; Zhang, Y.; Wang, C. R.; Shu, C. Y.; Hong, H. et al. Biodegradable, hydrogen peroxide, and glutathione dual responsive nanoparticles for potential programmable paclitaxel release. *J. Am. Chem. Soc.* **2018**, *140*, 7373–7376.

[22] Feng, H.; Qian, Z. S. Functional carbon quantum dots: A versatile platform for chemosensing and biosensing. *Chem. Rec.* **2018**, *18*, 491–505.

[23] Roy, P.; Chen, P. C.; Periasamy, A. P.; Chen, Y. N.; Chang, H. T. Photoluminescent carbon nanodots: Synthesis, physicochemical properties and analytical applications. *Mater. Today* **2015**, *18*, 447–458.

[24] Yang, S. T.; Cao, L.; Luo, P. G.; Lu, F. S.; Wang, X.; Wang, H. F.; Meziani, M. J.; Liu, Y. F.; Qi, G.; Sun, Y. P. Carbon dots for optical imaging *in vivo*. *J. Am. Chem. Soc.* **2009**, *131*, 11308–11309.

[25] Huang, P.; Lin, J.; Wang, X. S.; Wang, Z.; Zhang, C. L.; He, M.; Wang, K.; Chen, F.; Li, Z. M.; Shen, G. X. et al. Light-triggered theranostics based on photosensitizer-conjugated carbon dots for simultaneous enhanced-fluorescence imaging and photodynamic therapy. *Adv. Mater.* **2012**, *24*, 5104–5110.

[26] Du, J. J.; Xu, N.; Fan, J. L.; Sun, W.; Peng, X. J. Carbon dots for *in vivo* bioimaging and theranostics. *Small* **2019**, *15*, 1805087.

[27] Zheng, M.; Ruan, S. B.; Liu, S.; Sun, T. T.; Qu, D.; Zhao, H. F.; Xie, Z. G.; Gao, H. L.; Jing, X. B.; Sun, Z. C. Self-targeting fluorescent carbon dots for diagnosis of brain cancer cells. *ACS Nano* **2015**, *9*, 11455–11461.

[28] Opacic, T.; Paefgen, V.; Lammers, T.; Kiessling, F. Status and trends in the development of clinical diagnostic agents. *Wiley Interdiscip. Rev. Nanomed. Nanobiotechnol.* **2017**, *9*, e1441.

[29] Aherne, G. W.; James, S. L.; Marks, V. The radioiodination of bleomycin using iodogen. *Clin. Chim. Acta* **1982**, *119*, 341–343.

[30] Spetz, J.; Rudqvist, N.; Forssell-Aronsson, E. Biodistribution and dosimetry of free ^{211}At, ^{125}I^{-} and ^{131}I^{-} in rats. *Cancer Biother. Radiopharm.* **2013**, *28*, 657–664.

[31] Cranley, K.; Bell, T. K. ^{125}I thyroid intakes: Consideration of thyroid radiation dose, and air and water concentration limits. *Int. J. Appl. Radiat. Isot.* **1979**, *30*, 161–163.

[32] Zhu, A. Z.; Yoon, Y.; Liang, Z. X.; Voll, R.; Goodman, M. E.; Goodman, M. M.; Shim, H. Abstract 5227: Detection of metastatic potential by a novel small molecule F-18 PET imaging agent. *Cancer Res.* **2011**, *71*, 5227.

[33] Foss, C. A.; Mease, R. C.; Fan, H.; Wang, Y. H.; Ravert, H. T.; Dannals, R. F.; Olszewski, R. T.; Heston, W. D.; Kozikowski, A. P.; Pomper, M. G. Radiolabeled small-molecule ligands for prostate-specific membrane antigen: *In vivo* imaging in experimental models of prostate cancer. *Clin. Cancer Res.* **2005**, *11*, 4022–4028.

[34] Mankoff, D. A.; Link, J. M.; Linden, H. M.; Sundararajan, L.; Krohn, K. A. Tumor receptor imaging. *J. Nucl. Med.* **2008**, *49 Suppl 2*, 149S–163S.

[35] Tang, S. H.; Peng, C. Q.; Xu, J.; Du, B. J.; Wang, Q. X.; Vinluan III, R. D.; Yu, M.X.; Kim, M. J.; Zheng, J. Tailoring renal clearance and tumor targeting of ultrasmall metal nanoparticles with particle density. *Angew. Chem., Int. Ed.* **2016**, *55*, 16039–16043.

[36] Zhao, R. B.; Keen, L.; Kong, X. D. Clinical translation and safety regulation of nanobiomaterials In *Nanobiomaterials: Classification, Fabrication and Biomedical Applications*. Wang X. M.; Ramalingam M.; Kong, X. D., Eds.; Wiley Germany: Verlag, 2017; pp 459–479.